Frontiers of Information Technology & Electronic Engineering
www.jzus.zju.edu.cn; engineering.cae.cn; www.springerlink.com
ISSN 2095-9184 (print); ISSN 2095-9230 (online)
E-mail: jzus@zju.edu.cn

Target parameter estimation for OTFS-integrated radar and communications based on sparse reconstruction preprocessing*

Zhenkai ZHANG†‡, Xiaoke SHANG, Yue XIAO

Ocean College, Jiangsu University of Science and Technology, Zhenjiang 212003, China

†E-mail: zhangzhenkai@just.edu.cn

Received July 9, 2023; Revision accepted Nov. 24, 2023; Crosschecked Apr. 20, 2024

Abstract: Orthogonal time–frequency space (OTFS) is a new modulation technique proposed in recent years for high Doppler wireless scenes. To solve the parameter estimation problem of the OTFS-integrated radar and communications system, we propose a parameter estimation method based on sparse reconstruction preprocessing to reduce the computational effort of the traditional weighted subspace fitting (WSF) algorithm. First, an OTFS-integrated echo signal model is constructed. Then, the echo signal is transformed to the time domain to separate the target angle from the range, and the range and angle of the detected target are coarsely estimated by using the sparse reconstruction algorithm. Finally, the WSF algorithm is used to refine the search with the coarse estimate at the center to obtain an accurate estimate. The simulations demonstrate the effectiveness and superiority of the proposed parameter estimation algorithm.

Key words: Integrated radar and communications system; Orthogonal time–frequency space; Target parameter estimation; Sparse reconstruction; Weighted subspace fitting

https://doi.org/10.1631/FITEE.2300462 **CLC number:** TN953

1 Introduction

Radar and communication devices have been widely used in various fields (Yan et al., 2020). With the advent of the sixth-generation (6G) era, information transmission and radar detection are facing the challenge of scarce spectrum resources, and the integrated radar and communications system (IRCS) can solve this problem by using integrated waveforms for data communication and radar detection (Dokhanchi et al., 2019; Zheng et al., 2019). IRCS can also effectively reduce the size, energy consumption, and weight of the system while increasing the spectrum utilization (Hassanien et al., 2019; Zhang ZK et al., 2021), which makes it gradually become a hot issue for current research.

When communication waveforms are used to achieve IRCS, orthogonal frequency division multiplexing (OFDM) waveforms are mainly used. Many scholars have studied the applications of OFDM in radar, communication, and IRCS (Hakobyan and Yang, 2018; Li YC et al., 2020; Sanson et al., 2020). However, OFDM-integrated signals suffer from the loss of subcarrier orthogonality in high Doppler scenarios, generating severe intercarrier interference, thus leading to the deterioration of communication and radar performance (Franken et al., 2006). To overcome this problem, orthogonal time–frequency space (OTFS) was first proposed by Hadani et al. (2017a). Moreover, OTFS technology can be obtained by adding preprocessing and termination processing modules on top of

‡ Corresponding author

* Project supported by the National Natural Science Foundation of China (No. 61871203) and the Postgraduate Scientific Research and Innovation Projects of Jiangsu Province, China (No. KYCX23_3878)

ORCID: Zhenkai ZHANG, https://orcid.org/0000-0003-2439-0923; Xiaoke SHANG, https://orcid.org/0009-0002-5137-2835; Yue XIAO, https://orcid.org/0009-0008-9343-5367

existing multi-carrier systems (Farhang et al., 2018), which means that OTFS can be compatible with existing OFDM systems and can be more easily deployed in the beyond fifth-generation/sixth-generation (B5G/6G) era. OTFS not only has a high Doppler tolerance (Surabhi et al., 2019a), but also enables low-latency communication with a lower peak average power than that of OFDM signals (Surabhi et al., 2019b) and lower cyclic prefix requirements (Raviteja et al., 2019b). In addition, OTFS has a stronger ability to eliminate multipath effects and intersymbol interference suppression (Keskin et al., 2021). Hadani et al. (2017b) conducted a system-level simulation of OFDM and OTFS performance at various speeds under the fourth-generation (4G) long term evolution (LTE) configuration, and the results showed that OTFS had a better bit error rate performance than OFDM in high-speed mobile scenarios. It was found that OTFS can achieve a performance gain of about 5 dB compared to OFDM, and that the OTFS system performance was further improved with increasing subcarrier spacing.

In daily life, whether it is the connected car or intelligent Internet of Things (IoT) and other environments, it is particularly important for devices to realize information interaction while sensing the surrounding environment (Xue et al., 2017). In the two-dimensional (2D) plane, the position of the target can be initially determined by obtaining the angle and distance of the detection target (Patole et al., 2017). At present, scholars' research on OTFS technology in communication has been relatively mature, but there is less research on the application of OTFS technology to radar detection or even IRCS. In Raviteja et al. (2019a), OTFS was applied to the radar system for the first time, and the delay–Doppler domain matching filter algorithm was proposed to detect the target speed and distance. They proved the feasibility and effectiveness of OTFS for radar detection and showed that the OTFS radar system's speed detection accuracy was significantly higher than that of the OFDM radar system. Gaudio et al. (2020a) applied OTFS to IRCS, deduced the Cramer–Rao lower bound (CRLB) for OTFS signal radar target parameter estimation, and used maximum likelihood (ML) estimation to obtain parameter values in the single target case. In Gaudio et al. (2020b), the OTFS-integrated signal was extended to a multi-input multi-output (MIMO) integrated system, and the ML estimation algorithm was used to achieve multi-target radar detection and parameter estimation in the case of separable angle, delay, and Doppler domains. Inspired by the compressed sampling of compressed sensing, Liu et al. (2021) used prior information to cut the observation matrix to reduce computational complexity and then carried out three-dimensional (3D) coupled sparse Bayesian learning for parameter estimation in multi-target scenes. Li SY et al. (2022) proposed an integrated system based on spatially spread orthogonal time frequency space (SS-OTFS), designed the angle-of-arrival (AOA) estimation algorithm using the radar sensing matrix structure, and investigated the power allocation problem of the system. The traditional algorithms for the joint estimation of angle and delay, to achieve signal processing, include mainly the multiple signal classification (MUSIC) algorithm (Shi et al., 2019), the weighted subspace fitting (WSF) algorithm (Wang et al., 2021), the ML algorithm (Zhang FQ et al., 2020), and the compressed sensing (CS) algorithm (Zheng and Wang, 2017; Rahman et al., 2020). However, all these methods require complex computational processes such as matrix decomposition, optimization, and search, and have high computational complexity.

Range and angle estimation of radar communication integrated echo signals is essential to improve radar perception of the surroundings and target localization performance. Array processing algorithms can be used for the parameter estimation of OTFS-integrated systems and, in general, WSF algorithms can handle coherent signals with optimal performance (Ottersten et al., 1992). To solve the problem of the large computational effort of the WSF algorithm, in this paper we propose a method based on sparse reconstruction preprocessing. First, the sparse reconstruction algorithm uses a coarse grid to obtain coarse estimates of angles and ranges, and then the WSF algorithm is used to perform accurate estimation around the coarse estimates on the search space. The dimension of the received signal is reduced in the coarse estimation to avoid the problem of information redundancy in the 2D dictionary matrix, and WSF is used for accurate estimation to improve the estimation accuracy. The advantages of this processing are that it enables the WSF algorithm to guarantee the parameter estimation with high accuracy, and that it avoids an unnecessary

grid search, which greatly reduces the computational complexity.

2 Signal model

2.1 OTFS-integrated transmission signal

In this study, we consider the use of a uniform line array (ULA), which has an array element number N_a, a ULA element spacing d, and elements each transmitting an OTFS radar communication integrated waveform. For better integration with the existing system, the OTFS system based on OFDM is adopted (Farhang et al., 2018). At the sending end, the data symbol $x_{k,l}$ (k=0, 1, ⋯, N−1; l=0, 1, ⋯, M−1) is placed on the N×M 2D plane, which is called the delay–Doppler plane. This plane is represented as $\Gamma=\{(k/(N\Delta f),\ l/(MT))\}$, where k is the index in the delay dimension, l is the index in the Doppler dimension, and T denotes the period. The transmitter first uses the inverse symplectic finite Fourier transform (ISFFT) to convert $x_{k,l}$ in the delay–Doppler domain to $X_{n,m}$ in the time–frequency domain. This is given by

$$X_{n,m}=\frac{1}{\sqrt{NM}}\sum_{l=0}^{M-1}\sum_{k=0}^{N-1}x_{k,l}\exp\left(\mathrm{j}2\pi\left(\frac{ml}{M}-\frac{nk}{N}\right)\right). \quad (1)$$

Then, a continuous time signal $s_1(t)$ is generated by the Heisenberg transform, as follows:

$$s_1(t)=\sum_{m=0}^{M-1}\sum_{n=0}^{N_c-1}X_{n,m}\,g_{tx}\left(t-mT_s\right)\exp\left(\mathrm{j}2\pi n\Delta f\left(t-mT_s\right)\right), \quad (2)$$

where the communication data sent on the n^{th} subcarrier of the m^{th} OTFS symbol are denoted by $X_{n,m}$, N_c is the number of subcarriers, $g_{tx}(\cdot)$ denotes the pulse function of the emission, and T_s is the symbol period, T_s=T_{cp}+T_u, with T_{cp} being the cyclic prefix time and T_u the time duration of the valid data on the OTFS symbol. To ensure that the individual subcarriers are orthogonal to each other, it is necessary to make T_u=1/Δf (Δf is the subcarrier frequency interval), and the total frame duration is T_f=MT_s.

In this study, a multi-symbol multi-pulse OTFS radar communication integrated signal is chosen; i.e., multiple sub-pulses belonging to the same pulse are sent. The baseband signal can be obtained as

$$s(t)=\sum_{p=0}^{P-1}\sum_{m=0}^{M-1}\sum_{n=0}^{N_c-1}X(n,m,p)\,g_{tx}\left(t-mT_s-pT_p\right)\cdot\exp\left(\mathrm{j}2\pi n\Delta f\left(t-mT_s-pT_p\right)\right), \quad (3)$$

where T_p is the pulse repetition period, P is the number of pulses, and $X(n,m,p)$ is the communication data information represented by the n^{th} subcarrier on the m^{th} symbol of the p^{th} pulse.

The baseband signal is up-converted to a transmit signal with a carrier frequency of f_c:

$$c(t)=s(t)\exp\left(\mathrm{j}2\pi f_c t\right). \quad (4)$$

2.2 Receiving signal model

Assuming an observation scenario for this system where the signal transmission is line-of-sight (LOS), the echo signal reflected by K targets with a range of R_k and an angle of θ_k (k=1, 2, ⋯, K) is $r(t)$. Under narrowband conditions, the expression for the OTFS radar communication integrated echo signal received by the array antenna after scattering from K targets is

$$r(t)=\sum_{k=1}^{K}h_k\exp(-\mathrm{j}2\pi N_a d\sin\theta_k/\lambda)\,s(t-\tau_k)\cdot\exp\left(\mathrm{j}2\pi f_c(t-\tau_k)\right)+n(t), \quad (5)$$

where τ_k is the delay, h_k is the transmission fading factor of the k^{th} target, λ is the signal wavelength, and $n(t)$ is the Gaussian white noise in the echo signal.

The echo signal is down-converted and the received echo signal is expressed as

$$r(t)=\sum_{k=1}^{K}h_k\exp(-\mathrm{j}2\pi N_a d\sin\theta_k/\lambda)\cdot s(t-\tau_k)\exp(-\mathrm{j}2\pi f_c\tau_k)+\bar{n}(t), \quad (6)$$

where $\bar{n}(t)$ is the noise after frequency conversion. The echo signal is sampled and discretized, t=iT_u/N_c+mT_s+pT_p (i=0, 1, ⋯, N_c−1), and the sampling frequency is f_s=$N_c\Delta f$. The signal is narrowband and, for simplicity, the discrete signal after the constant term $\exp\left(-\mathrm{j}2\pi f_c\frac{2R_k}{c}\right)$ is ignored as follows:

$$r_{m,p}(i)=\sum_{k=1}^{K}\sum_{n=0}^{N_c-1}h_k X(n,m,p)\exp(-\mathrm{j}2\pi N_a d\sin\theta_k/\lambda)\cdot\exp\left(\mathrm{j}2\pi n\Delta f\frac{iT_u}{N_c}\right)\exp\left(-\mathrm{j}2\pi n\Delta f\frac{2R_k}{c}\right)+\bar{n}_{m,p}(i), \quad (7)$$

where c is the speed of light in free space, and $\bar{n}_{m,p}(i)=n(iT_u/N_c+mT_s+pT_p)$ is the sampling of the noise.

The echo signal received by the system, written in the matrix form, is as follows:

$$\boldsymbol{R}_p=\sum_{k=1}^{K}h_k\boldsymbol{X}_p\boldsymbol{B}_k\boldsymbol{F}^{\mathrm{H}}\boldsymbol{\Gamma}_k+\bar{\boldsymbol{N}}_p, \tag{8}$$

where $\overline{\boldsymbol{N}}_p$ is the matrix form of the received Gaussian white noise, $\boldsymbol{X}_p$ is the communication data matrix,

$$\boldsymbol{B}_k=\left[1,\exp\left(\frac{-\mathrm{j}2\pi d\sin\theta_k}{\lambda}\right),\cdots,\exp\left(\frac{-\mathrm{j}2\pi\left(N_a-1\right)d\sin\theta_k}{\lambda}\right)\right]^{\mathrm{T}} \tag{9}$$

represents the array guidance vector of the antenna transmitting model arriving at the receiving end, $\boldsymbol{F}^{\mathrm{H}}$ is the Fourier transform conjugate matrix, and $\boldsymbol{\Gamma}_k=\mathrm{diag}(\boldsymbol{\beta}_k)$ with

$$\boldsymbol{\beta}_k=\left[1,\exp\left(-\mathrm{j}2\pi\Delta f\left(\frac{2R_k}{c}\right)\right),\cdots,\exp\left(-\mathrm{j}2\pi\left(N_c-1\right)\Delta f\left(\frac{2R_k}{c}\right)\right)\right]^{\mathrm{T}} \tag{10}$$

being the delay vector.

For the radar communication integrated signal, the communication information carried in the echo signal will affect the detection performance of the system. For radars, the communication information carried by the echo signal can be known if the transmitted waveform is known, that is, the communication data $X(n,m,p)$ of the OTFS-integrated signal. To eliminate the impact of communication information on the detection performance and achieve estimation with higher accuracy, the communication information in the received data can be compensated for directly before radar signal processing. First, the received echo signal is multiplied with the discrete Fourier transform matrix $\boldsymbol{F}^{-1}$ to change the signal to the frequency domain, and then the inverse matrix of the information matrix $\boldsymbol{X}_p^{-1}$ is used to compensate for the communication information of Eq. (8):

$$\boldsymbol{F}^{-1}\boldsymbol{R}_p\boldsymbol{X}_p^{-1}=\sum_{k=1}^{K}h_k\boldsymbol{B}_k\boldsymbol{\Gamma}_k+\boldsymbol{F}^{-1}\bar{\boldsymbol{N}}_p\boldsymbol{X}_p^{-1}. \tag{11}$$

Define the expressions for the p^{th} received pulse matrix and the noise matrix after preprocessing as $\tilde{\boldsymbol{R}}_p=\boldsymbol{F}\boldsymbol{R}_p\boldsymbol{X}_p^{-1}$ and $\tilde{\boldsymbol{N}}_p=\boldsymbol{F}\bar{\boldsymbol{N}}_p\boldsymbol{X}_p^{-1}$, respectively.

The received matrices are combined by column and, after information compensation and rearrangement, the matrix contains only the angle and range information of the radar detection target to be estimated. Define the expression of the receive model as follows:

$$\tilde{\boldsymbol{R}}=\tilde{\boldsymbol{A}}\tilde{\boldsymbol{H}}+\tilde{\boldsymbol{N}}, \tag{12}$$

where

$$\tilde{\boldsymbol{A}}=\left[\tilde{\boldsymbol{a}}\left(R_1,\theta_1\right),\tilde{\boldsymbol{a}}\left(R_2,\theta_2\right),\cdots,\tilde{\boldsymbol{a}}\left(R_k,\theta_k\right)\right], \tag{13}$$

$$\tilde{\boldsymbol{a}}\left(R_k,\theta_k\right)=\boldsymbol{B}_k\otimes\boldsymbol{\beta}_k, \tag{14}$$

$$\tilde{\boldsymbol{H}}=\left[h_1,h_2,\cdots,h_k\right]^{\mathrm{T}}. \tag{15}$$

The parameter matrix containing the angles and ranges is expressed as

$$\boldsymbol{\Phi}=\begin{bmatrix}\boldsymbol{\Phi}_1\\ \boldsymbol{\Phi}_2\\ \vdots\\ \boldsymbol{\Phi}_{N_a}\end{bmatrix}=\tilde{\boldsymbol{A}}\tilde{\boldsymbol{H}}. \tag{16}$$

3 OTFS-integrated target parameter estimation based on sparse reconstruction preprocessing

3.1 WSF algorithm

The WSF algorithm is considered to be one of the most commonly applied and reliable parameter estimation algorithms in array signal processing, and it is known from the parameter selection criterion of the WSF algorithm that the algorithm can handle signals with correlation. The specific algorithm proof and derivation can be found in Ottersten et al. (1993).

To obtain the angle and range data of the detection target, the covariance matrix of the received narrowband signal vector in Eq. (12) needs to be found as

$$\boldsymbol{R}_{\tilde{R}}=\frac{1}{M}\tilde{\boldsymbol{R}}\tilde{\boldsymbol{R}}^{\mathrm{H}}. \tag{17}$$

Eigenvalue decomposition of the resulting covariance matrix is as follows:

$$\boldsymbol{R}_{\tilde{R}}=\boldsymbol{U}_{\tilde{R}}\boldsymbol{\Sigma}_{\tilde{R}}\boldsymbol{U}_{\tilde{R}}^{\mathrm{H}}=\boldsymbol{U}_{\mathrm{S}}\boldsymbol{\Sigma}_{\mathrm{S}}\boldsymbol{U}_{\mathrm{S}}^{\mathrm{H}}+\boldsymbol{U}_{\mathrm{N}}\boldsymbol{\Sigma}_{\mathrm{N}}\boldsymbol{U}_{\mathrm{N}}^{\mathrm{H}}, \tag{18}$$

where $\boldsymbol{U}_{\mathrm{S}}$ and $\boldsymbol{U}_{\mathrm{N}}$ are the eigenvectors corresponding to the signal subspace and noise subspace respectively, and $\boldsymbol{\Sigma}_{\mathrm{S}}$ and $\boldsymbol{\Sigma}_{\mathrm{N}}$ are the eigenvalue diagonal matrices.

In the ideal case, the eigenvalues after covariance eigendecomposition are mutually orthogonal and linearly independent; the signal subspace is a linear subspace of the array manifold tensor, $\mathrm{span}\{\boldsymbol{U}_{\mathrm{S}}\}=\mathrm{span}\{\tilde{\boldsymbol{A}}\}$, and there exists a full-rank matrix $\boldsymbol{T}$ such that

$$\boldsymbol{U}_{\mathrm{S}}=\tilde{\boldsymbol{A}}\boldsymbol{T}, \tag{19}$$

$$\boldsymbol{T}=\boldsymbol{R}_{\mathrm{S}}\boldsymbol{A}^{\mathrm{H}}\boldsymbol{U}_{\mathrm{S}}\left(\boldsymbol{\Sigma}_{\mathrm{S}}-s^2\boldsymbol{I}\right)^{-1}, \tag{20}$$

where $\boldsymbol{R}_{\mathrm{S}}$ is the covariance matrix of the signal matrix and $\boldsymbol{I}=\boldsymbol{U}_{\mathrm{S}}^{\mathrm{H}}\boldsymbol{U}_{\mathrm{S}}$. The problem of spatial mismatch arises when there is noise interference in the signal; thus, WSF is used to construct a fitting relationship to obtain a matrix that allows Eq. (19) to hold, and to ensure that the two subspaces fit best under least squares:

$$\{\boldsymbol{\theta},\hat{\boldsymbol{T}}\}=\min\left\|\boldsymbol{U}_{\mathrm{S}}-\tilde{\boldsymbol{A}}\hat{\boldsymbol{T}}\right\|_{\mathrm{F}}^2. \tag{21}$$

In the above equation, $\boldsymbol{\theta}=[R_1, R_2, \cdots, R_K, \theta_1, \theta_2, \cdots, \theta_K]^{\mathrm{T}}$ represents the range and angle parameters of the detection target to be estimated and $\hat{\boldsymbol{T}}$ is an auxiliary parameter. Therefore, by fixing the value of $\tilde{\boldsymbol{A}}$, a least squares fit solution can be obtained as

$$\hat{\boldsymbol{T}}=(\tilde{\boldsymbol{A}}^{\mathrm{H}}\tilde{\boldsymbol{A}})^{-1}\tilde{\boldsymbol{A}}^{\mathrm{H}}\boldsymbol{U}_{\mathrm{S}}=\tilde{\boldsymbol{A}}^{+}\boldsymbol{U}_{\mathrm{S}}. \tag{22}$$

Substituting the least squares fit solution (22) for $\hat{\boldsymbol{T}}$ into Eq. (21) yields

$$\begin{aligned}\boldsymbol{\theta}&=\min\left\|\boldsymbol{U}_{\mathrm{S}}-\tilde{\boldsymbol{A}}\tilde{\boldsymbol{A}}^{+}\boldsymbol{U}_{\mathrm{S}}\right\|_{\mathrm{F}}^2\\&=\min\mathrm{tr}\left\{\boldsymbol{P}_{\tilde{A}}^{\perp}\boldsymbol{U}_{\mathrm{S}}\boldsymbol{U}_{\mathrm{S}}^{\mathrm{H}}\right\}=\max\mathrm{tr}\left\{\boldsymbol{P}_{\tilde{A}}\boldsymbol{U}_{\mathrm{S}}\boldsymbol{U}_{\mathrm{S}}^{\mathrm{H}}\right\},\end{aligned} \tag{23}$$

where $\boldsymbol{P}_{\tilde{A}}=(\tilde{\boldsymbol{A}}^{\mathrm{H}}\tilde{\boldsymbol{A}})^{-1}\tilde{\boldsymbol{A}}^{\mathrm{H}}$. It is evident that the answer to the signal subspace fit is the optimization issue of Eq. (22), and a generalization of Eq. (21) yields the fitting problem using the matrix $\boldsymbol{W}$ to weight the signal subspace, which can be written as

$$\{\boldsymbol{\theta},\hat{\boldsymbol{T}}\}=\min\left\|\boldsymbol{U}_{\mathrm{S}}\boldsymbol{W}^{1/2}-\tilde{\boldsymbol{A}}\hat{\boldsymbol{T}}\right\|_{\mathrm{F}}^2. \tag{24}$$

The solution for the estimated detection target parameters can be obtained as

$$\boldsymbol{\theta}=\min\mathrm{tr}\left\{\boldsymbol{P}_{\tilde{A}}^{\perp}\boldsymbol{U}_{\mathrm{S}}\boldsymbol{W}\boldsymbol{U}_{\mathrm{S}}^{\mathrm{H}}\right\}=\max\mathrm{tr}\left\{\boldsymbol{P}_{\tilde{A}}\boldsymbol{U}_{\mathrm{S}}\boldsymbol{W}\boldsymbol{U}_{\mathrm{S}}^{\mathrm{H}}\right\}, \tag{25}$$

when the signal subspace weighting matrix satisfies

$$\boldsymbol{W}_{\mathrm{S\,opt}}=\left(\boldsymbol{\Sigma}_{\mathrm{S}}-\sigma^2\boldsymbol{I}\right)^2\boldsymbol{\Sigma}_{\mathrm{S}}^{-1}. \tag{26}$$

The resultant values of the parameter estimation of the WSF algorithm for the optimal weights can be obtained by solving Eq. (25). In this study, to further reduce the difficulty in solving this multidimensional optimal problem, an alternate projection transform is used to convert the complex multidimensional optimal search problem into multiple simple one-dimensional (1D) optimization problems. In this solution process, the expression for the k^{th} detection target at the moment of the $(i+1)^{\mathrm{th}}$ iteration is

$$\left(\hat{R}_k^{i+1},\theta_k^{i+1}\right)=\max\mathrm{tr}\left\{\boldsymbol{P}_{\tilde{A}_k^i}\boldsymbol{U}_{\mathrm{S}}\boldsymbol{W}_{\mathrm{S\,opt}}\boldsymbol{U}_{\mathrm{S}}^{\mathrm{H}}\right\}, \tag{27}$$

where $\tilde{\boldsymbol{A}}_k^i=\left[\tilde{\boldsymbol{A}}_1^i, \tilde{\boldsymbol{A}}_2^i, \cdots, \tilde{\boldsymbol{A}}_k\right]$ represents a matrix in which the first $k-1$ columns contain the previously computed parameter vectors, and column k contains the corresponding vectors for the target parameters currently under estimation. The algorithm iterates for a total of K cycles to estimate the target parameters.

3.2 Preprocessing based on sparse reconstruction

The WSF algorithm of Eq. (25) requires a global search over range and angle, as K cycles of $NN_{\mathrm{a}}N_1N_{\mathrm{a1}}$ iterations are required in the search process, where the array stream length is NN_{a}, N_1 is the number of subgrids searched for range, and N_{a1} is the number of subgrids searched for angle; the search scope and complexity are too large. A sparse reconstruction method with good parameter estimation performance and resolution is presented below as a way to narrow the search and reduce the computational effort. According to the idea of sparse reconstruction, the 2D spatial plane of the radar detection target is considered in the ordinary OTFS narrowband array signal model, and the detection ranges of range and angle are divided into rs and ts grid points, respectively. Let the set $\{\tilde{\theta}_1, \tilde{\theta}_2, \cdots, \tilde{\theta}_{\mathrm{ts}}\}$ and the set $\{\tilde{r}_1, \tilde{r}_2, \cdots, \tilde{r}_{\mathrm{rs}}\}$ respectively contain angle and range information that can cover all possible positions of the detection target, of which there are only K real existing target points, which is much smaller

than the number of divided grids, so we can regard the range and angle spectrum as sparse. To address the problem that the 2D grid division in the sparse representation model of the received signal increases the difficulty of signal reconstruction, in this study we convert the 2D reconstruction into 1D reconstruction to reduce the complexity of the algorithm.

For Eq. (16), the elements of row n_a (n_a=1, 2, ⋯, N_a) of the parameter matrix $\boldsymbol{\Phi}$ are written as Eq. (28) (on the bottom of this page).

Each element of the row vector contains information about the parameters of the detection target, the same phase caused by the detection angle, and a fixed phase difference generated by the detection range. A Fourier transform of Eq. (28) converts the data to the time domain:

$$X_{\text{row}}(l)=\frac{1}{N}\sum_{k=1}^{K}h_k\exp\left(-\text{j}2\pi\left(N_{\text{c}}-1\right)\Delta f\left(\frac{2R_k}{c}\right)\right)\cdot\sum_{n=0}^{N-1}\exp\left(\text{j}2\pi n\left(\frac{l}{N}-\Delta f\left(\frac{2R_k}{c}\right)\right)\right). \tag{29}$$

According to the above equation, it can be seen that the magnitude of the time-domain data vector $\boldsymbol{X}_{\text{row}}$ can be taken to its maximum value when the index is $l_{\max}=N\Delta f\tau$. Substituting the index at the maximum value into Eq. (29), we can obtain

$$X_{\text{row}}\left(l_{\max}\right)=\sum_{k=1}^{K}h_k\Delta\exp\left(-\text{j}2\pi n_{\text{a}}d\sin\theta_k/\lambda\right), \tag{30}$$

where $\Delta=\frac{1}{N}\sum_{n=0}^{N-1}\exp(\text{j}2\pi n\delta/N)$ is the error term with $0<\delta<1$; that is, when the row vector takes the maximum value, the phase change information caused by the delay has been eliminated and only the target angle information remains in the parameter information matrix. After the above analysis, the inverse Fourier transform can be performed in Eq. (16) by row, and the data with the largest magnitude in the transformed matrix will be presented and written as

$$\boldsymbol{X}_{\max}=\tilde{\boldsymbol{A}}\begin{bmatrix}\zeta_1\\ \zeta_2\\ \vdots\\ \zeta_K\end{bmatrix}, \tag{31}$$

where $\zeta_i=h_i\Delta$ (i=1, 2, ⋯, K), and the separation of the range and angle parameters of the detection target is completed. A 2D to 1D downscaling of Eq. (31) is performed to expand the guide vector:

$$\boldsymbol{X}_{\max}=\tilde{\boldsymbol{A}}\boldsymbol{\zeta}, \tag{32}$$

where $\tilde{\boldsymbol{A}}$ is a redundant dictionary matrix and $\boldsymbol{\zeta}$ contains K non-zero elements, which appear only when the angle is the true angle of the detection target, with each non-zero element corresponding to a target parameter.

For Eq. (32), the l_1 parametric constraint function is constructed to obtain information on the angle parameters of the detection target:

$$\begin{aligned}&\min\left\|\boldsymbol{\zeta}\right\|_1\\ &\text{s.t.}\ \left\|\boldsymbol{X}_{\max}-\tilde{\boldsymbol{A}}\boldsymbol{\zeta}\right\|_2<\varepsilon.\end{aligned} \tag{33}$$

Problem (33) can be solved directly using the CVX software package. The angle corresponding to the column vector in $\tilde{\boldsymbol{A}}$, corresponding to the non-zero row in $\boldsymbol{\zeta}$, is the coarse estimate of the angle, i.e., $\left\{\tilde{\theta}_1,\tilde{\theta}_2,\cdots,\tilde{\theta}_K\right\}$, and the coarse estimate of the detection target's range $\hat{R}=i_{\max}c/(N\Delta f)$ can be obtained from the peak index.

3.3 Accurate estimation of OTFS integration target parameters

At this point, the initial estimates of the angle and range of the OTFS integration target have been obtained.

$$\boldsymbol{\Phi}_{n_{\text{a}}}=\begin{bmatrix}\sum_{k=1}^{K}h_k\exp\left(-\text{j}2\pi n_{\text{a}}d\sin\theta_k/\lambda\right)\\ \sum_{k=1}^{K}h_k\exp\left(-\text{j}2\pi n_{\text{a}}d\sin\theta_k/\lambda\right)\exp\left(-\text{j}2\pi\Delta f\left(\frac{2R_k}{c}\right)\right)\\ \vdots\\ \sum_{k=1}^{K}h_k\exp\left(-\text{j}2\pi n_{\text{a}}d\sin\theta_k/\lambda\right)\exp\left(-\text{j}2\pi\left(N_{\text{c}}-1\right)\Delta f\left(\frac{2R_k}{c}\right)\right)\end{bmatrix}^{\text{T}}. \tag{28}$$

In the sparse reconstruction method, the discrete Fourier transform is used to separate the angle and range information in the received signal of the array, the 2D dictionary matrix is reduced to a 1D dictionary matrix, and the complexity of the algorithm is reduced. However, the limitations of the discrete Fourier operation make the estimation accuracy low, and only the rough spectral peak positions of the detection target parameters can be obtained. The WSF algorithm uses this coarse estimate as the center for determining the search range, and the new search space range is further improved by a more refined subgrid division, with N_2 and N_{a2} being the updated numbers of subgrids searched for range and angle, respectively. Since the coarse estimate of the sparse reconstruction algorithm reduces the global search range of angles and ranges to a single region, WSF reduces unnecessary search steps, resulting in a significant reduction in the number of iterations. The steps of the integrated target parameter estimation algorithm based on sparse reconstruction preprocessing are given in Algorithm 1.

Algorithm 1 Integrated target parameter estimation algorithm based on sparse reconstruction preprocessing

1. Apply an inverse Fourier transform of the parameter matrix $\boldsymbol{\Phi}$ to obtain time-domain data
2. Put forward the data with the largest amplitude in the time-domain data matrix and write the data in the matrix form
3. Construct the l_1-parametric constraint function (33)
4. Use the CVX toolkit to obtain a coarse estimate of the angle
5. Use $\hat{R}=i_{\max}c/(N\Delta f)$ to find a rough estimate of the range
6. Update the search space for precise parameter estimation based on the coarse estimate of the detection target parameters obtained in step 5
7. Calculate the covariance matrix $\boldsymbol{R}_{\hat{R}}$ in Eq. (17)
8. Perform eigenvalue decomposition and ordering, and construct the signal subspace $\boldsymbol{U}_S$ in Eq. (19)
9. Compute the optimal value of the weighting matrix $\boldsymbol{W}_{S\,opt}$ using Eq. (26)
10. Initialize parameters k=1, i=1
11. Repeat
12. Update the search space for detecting the angle and range parameters of the target
13. Repeat
14. Update the matrix
15. Calculate and record the results
16. $i=i+1$
17. Until $i=N_2N_{a2}$
18. The location of the spectral peak is found, i.e., the parameters θ_k, R_k
19. $k=k+1$
20. Until $k=K$

4 Computer simulation analysis

In this section, the effectiveness of the proposed algorithm is simulated. Different methods and different metrics are applied to the simulations, and the superiority of the proposed algorithm is demonstrated with regard to the estimation error, theoretical error, and resolution in several ways. Considering the exact estimation in the MUSIC algorithm, the WSF algorithm, and the proposed algorithm, there is a process of angle and range grid search, and the estimation accuracy is related to the search grid density. We set the number of subgrids for range and angle division to $N_1=N_{a1}=16$, where the subgrids are expanded by one adjacent grid in the algorithm proposed in this study, as well as further subdivision with a fine fraction of 2. The OTFS radar communication integration parameters used for the simulation are set with reference to Raviteja et al. (2019a) and Gaudio et al. (2020a), as shown in Table 1.

Table 1 System parameters

Parameter	Symbol	Value
Carrier frequency	f_c	5.9 GHz
Number of OTFS symbols	M	8
Signal bandwidth	B	10 MHz
Number of subcarriers	N_c	16
Number of array elements	N_a	16
Number of pulses	P	16
Time duration of the valid data on the OTFS symbol	T_u	1.6 μs
Cyclic prefix time	T_{cp}	0.2 μs
Complete symbol period	T_s	1.8 μs
Pulse repetition period	T_p	100 μs

OTFS: orthogonal time–frequency space

4.1 Parameter estimation accuracy and compution time as influenced by SNR

The parameter estimation performances of the proposed algorithm, the ESPRIT algorithm, the MUSIC algorithm, and the conventional WSF algorithm with different signal-to-noise ratios (SNRs) are given in Fig. 1. The communication information is generated randomly

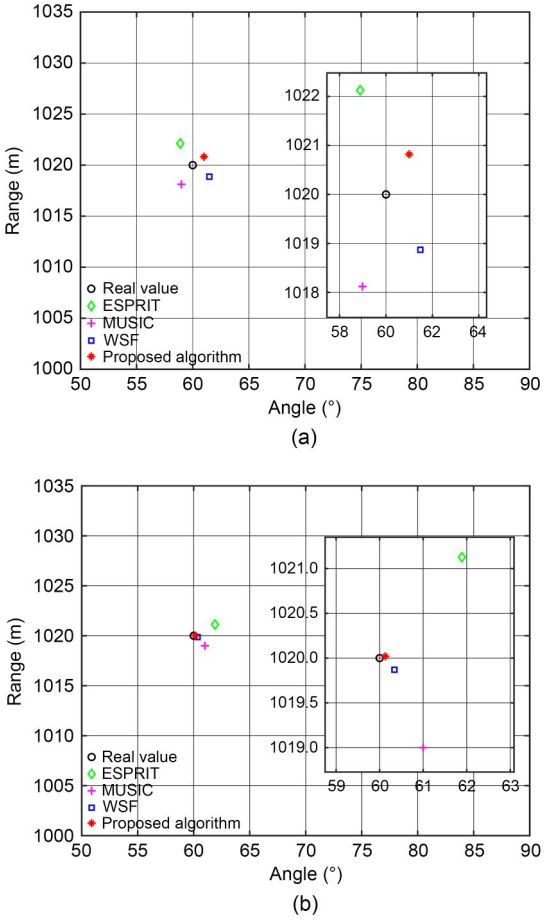

Fig. 1 Comparison of the target parameter estimation results for SNR= −5 dB (a) and SNR=5 dB (b) (SNR: signal-to-noise ratio)

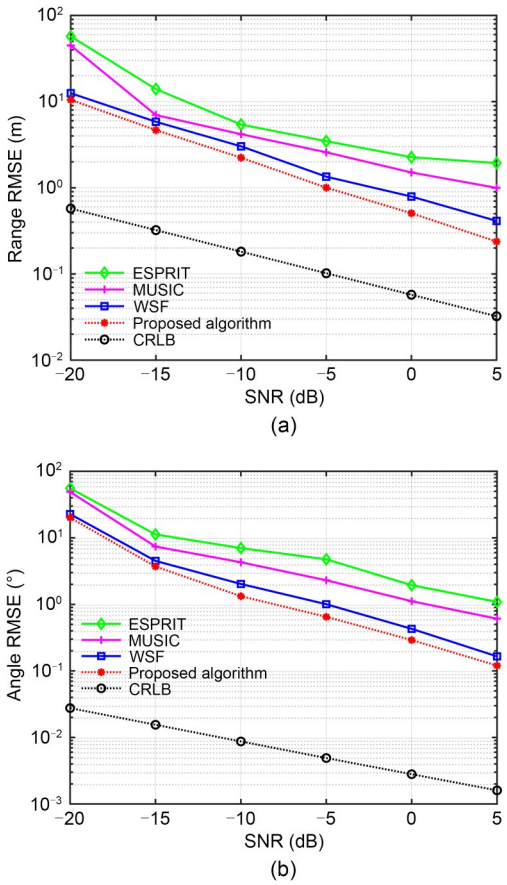

Fig. 2 Multi-target estimation performance versus SNR: (a) range estimation RMSE versus SNR; (b) angle estimation RMSE versus SNR (SNR: signal-to-noise ratio; RMSE: root mean square error)

and 16 quadrature amplitude modulation (16QAM) is used to generate the communication modulation information. The other simulation parameters are the same as in Table 1, and the radar detection target is set to be a single target at a range of 1020 m and an angle of 60°.

From Fig. 1, we can see that the algorithm in this study has more efficient estimation results compared to other algorithms for SNR, and that it has a higher estimation accuracy with smaller errors even at a small SNR.

Next, the accuracy of the parameter estimation of the proposed algorithm and the comparison algorithms is further investigated. To obtain the root mean square error (RMSE) shown in Fig. 2, the SNR increases from −20 to 5 dB with the incremental step of SNR being selected as 5 dB. The angle and range parameters for the three targets are set to (−45°, 900 m), (60°, 1040 m), and (80°, 1080 m), the other parameters are the same as those presented in Table 1, and the number of Monte Carlo simulations is set to 100. Fig. 2 reflects the parameter estimation errors for range and angle.

The simulation results shown in Fig. 2 further reflect the advantage of the proposed algorithm over the ESPRIT algorithm, MUSIC algorithm, and traditional WSF algorithm in terms of estimation accuracy. Although the estimation quality of all algorithms is improved with increasing SNR, the estimation performance of the proposed algorithm is better than those of the other algorithms and closer to the CRLB. ESPRIT has the worst estimation performance because this algorithm requires a certain phase difference between the received signals, and the phase difference cannot exceed a certain range; otherwise, it will lead to errors in angle estimation. The MUSIC algorithm outperforms the ESPRIT algorithm because

it uses the orthogonality of the array vector to the noise subspace to search for the spectral peaks of angle and range. Since WSF performs the fitting of the signal subspace, it performs better than MUSIC. However, since our proposed algorithm uses coarse estimation to obtain a more accurate search region and performs further subdivision of the subgrids, its estimation accuracy is higher than that of the WSF algorithm.

In terms of operation time, as shown in Fig. 3, the ESPRIT algorithm is numerical and therefore has the lowest operation time. The MUSIC algorithm requires a grid peak search of the spatial spectral function and therefore has a larger operation time than ESPRIT. The conventional WSF algorithm performs a large number of searches to maintain the estimation accuracy, thus resulting in the highest computation time. The running time of the proposed algorithm is less than that of the traditional WSF algorithm because of the lower computational complexity of the reduced-dimension sparse reconstruction algorithm, and the coarse estimate greatly reduces the unnecessary search intervals in the WSF algorithm, thus decreasing the number of iterations of the search and reducing the computation time of the proposed algorithm while maintaining the estimation reliability.

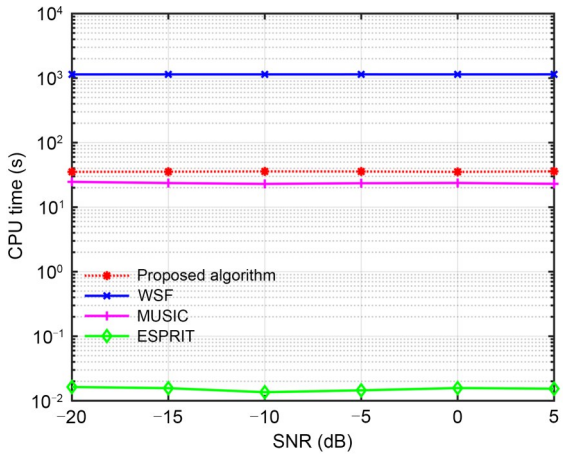

Fig. 3 Operation time versus SNR (SNR: signal-to-noise ratio; CPU: central processing unit)

4.2 Performance comparison with different numbers of subcarriers and array elements

In this subsection, the influence of the number of subcarriers and the number of array elements on the proposed algorithm and the comparison algorithms is analyzed. The number of array elements is fixed at 16, the number of subcarriers is taken as {4, 8, 16, 32, 64}, and the other parameters are the same as those in the simulation described in Section 4.1. Fig. 4 shows that the estimation accuracy of the algorithm is improved with the increase of the number of subcarriers; overall, the proposed algorithm has the highest estimation accuracy, and the quantity of subcarriers has a greater effect on the range estimation accuracy.

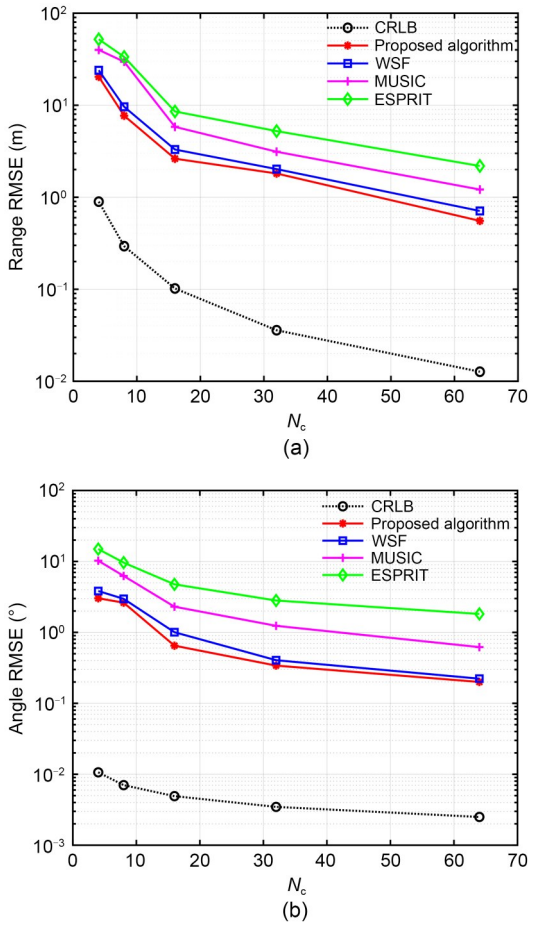

Fig. 4 Multi-target estimation performance versus the number of subcarriers N_c: (a) range estimation RMSE versus N_c; (b) angle estimation RMSE versus N_c (RMSE: root mean square error)

To investigate the influence of the number of array elements on the estimation performance of the method, the number of subcarriers is set to 16, the number of array elements is set to {4, 8, 16, 32, 64}, and the other parameters remain unchanged. According to the simulation results presented in Fig. 5, the

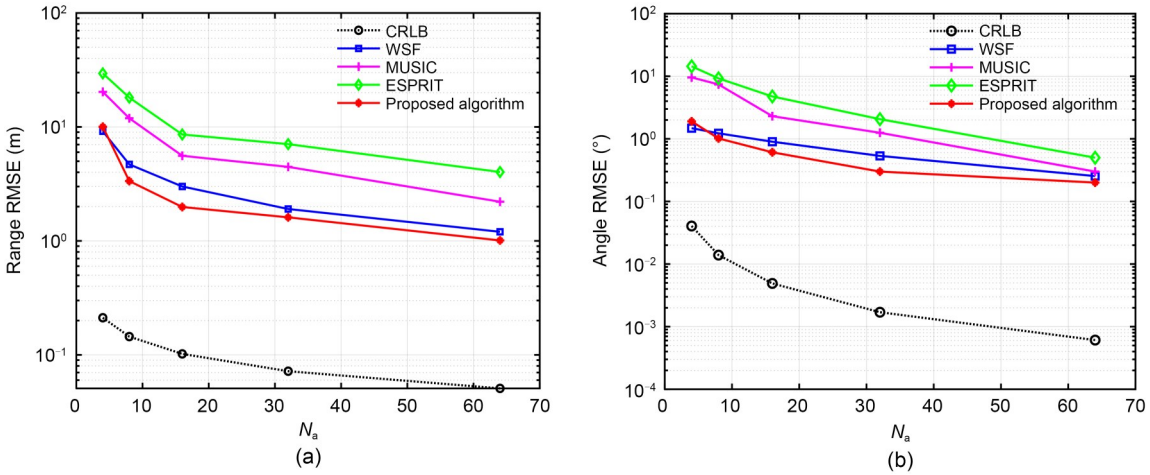

Fig. 5 Multi-target estimation performance versus the number of array elements N_a: (a) range estimation RMSE versus N_a; (b) angle estimation RMSE versus N_a (RMSE: root mean square error)

more antenna arrays of the OTFS radar communication integrated system there are, the better the algorithm's parameter estimation performance will be. The proposed algorithm has the best performance in estimating the angle and range parameters, and the number of array elements has a greater influence on angle estimation accuracy.

4.3 Resolution performance

To analyze and verify the angle resolution of the proposed algorithm for detecting targets, two target points are selected with a range of 1020 m and angles of 40° and 43°. In the range resolution simulations, two target points are selected with an angle of 40° and ranges of 1020 and 1023 m, and the echo SNR of the target is chosen to be 10 dB. To improve the resolution, the numbers of subcarriers and array elements are both set to 32, and the other simulation parameters are the same as those in Section 4.1.

Fig. 6 presents a spectrum plot comparing the other algorithms and the proposed algorithm to reflect their resolution performance in terms of angles. It can be seen that the ESPRIT algorithm has a large error in estimating the two targets when they are at adjacent angles; the MUSIC algorithm does not identify the two targets and detects only one target, with only one spectral peak in the spectrogram, and the estimated angle is approximately the middle of the two angles. This is due to the fact that both WSF and the proposed algorithm fit the orthogonal projection matrix of the array manifold matrix to the received signal subspace rather than the noise subspace, as in MUSIC. However, overall, the proposed algorithm has fewer search iterations and is able to reduce the complexity of the algorithm while maintaining the angle resolution. The same conclusion can be drawn in Fig. 7 in terms of range resolution.

To further visualize the resolution performance of the algorithm, a profile of the spectrum is plotted. The same conclusions can be drawn from Fig. 8 as were drawn from Figs. 6 and 7. It can be seen from Fig. 8 that the MUSIC algorithm, because of the 2D spatial smoothing, has a lower peak parametrization from the power spectrum profile, but forms only one spectral peak; it treats the neighboring targets as one target so that the targets cannot be distinguished or accurately estimated. In contrast, the proposed algorithm in this study can distinguish between two targets when they are at the same range or at the same angle, and the estimation errors for range and angle are smaller than those in other algorithms.

5 Conclusions

For the angle and range estimation problem of the OTFS-integrated radar and communications system, we have proposed a target parameter estimation algorithm based on sparse reconstruction preprocessing. First, the sparse reconstruction algorithm has been used to coarsely measure the angle and range of the detected target, and the search ranges of the range and

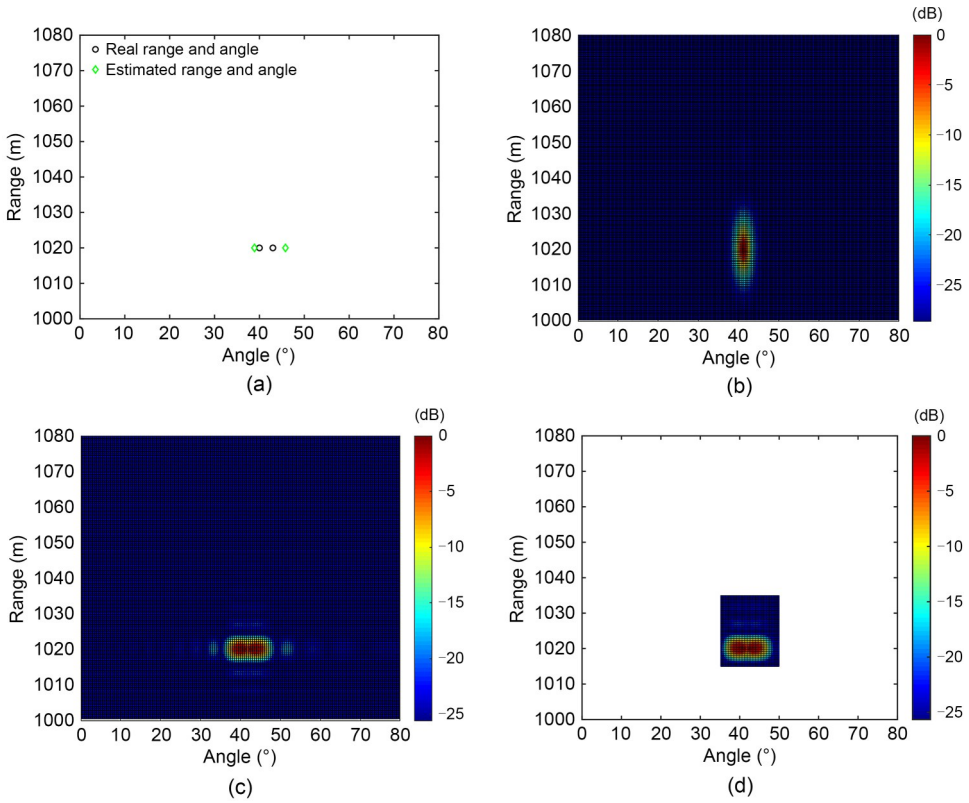

Fig. 6 Angle resolution images: (a) ESPRIT; (b) MUSIC; (c) WSF; (d) the proposed algorithm

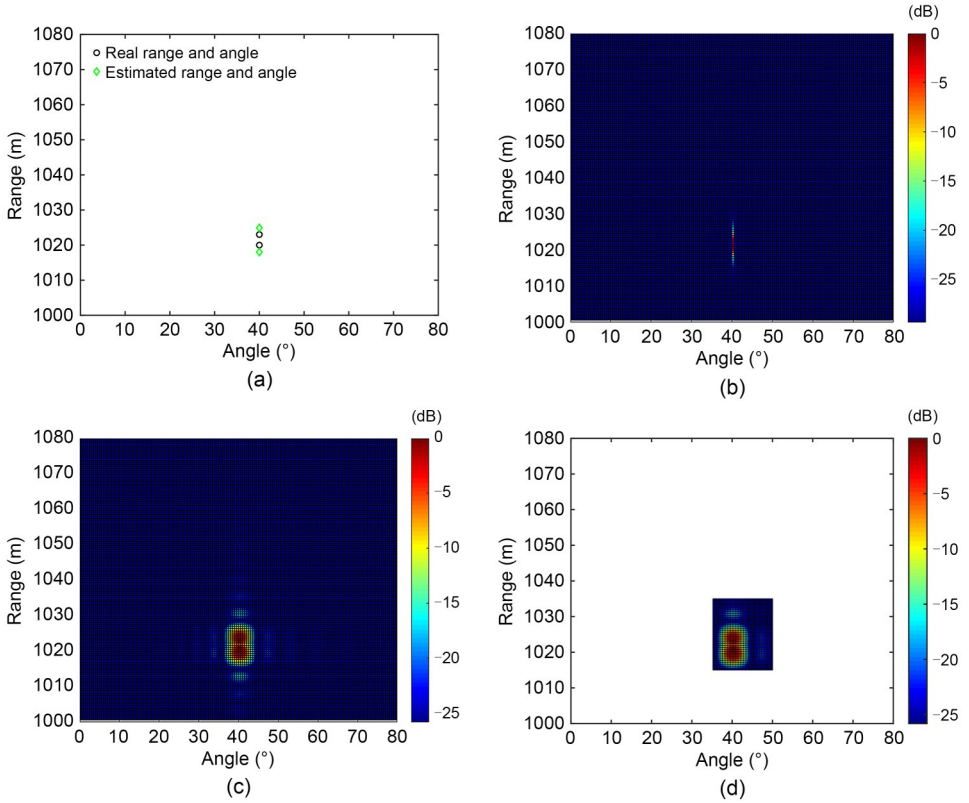

Fig. 7 Range resolution images: (a) ESPRIT; (b) MUSIC; (c) WSF; (d) the proposed algorithm

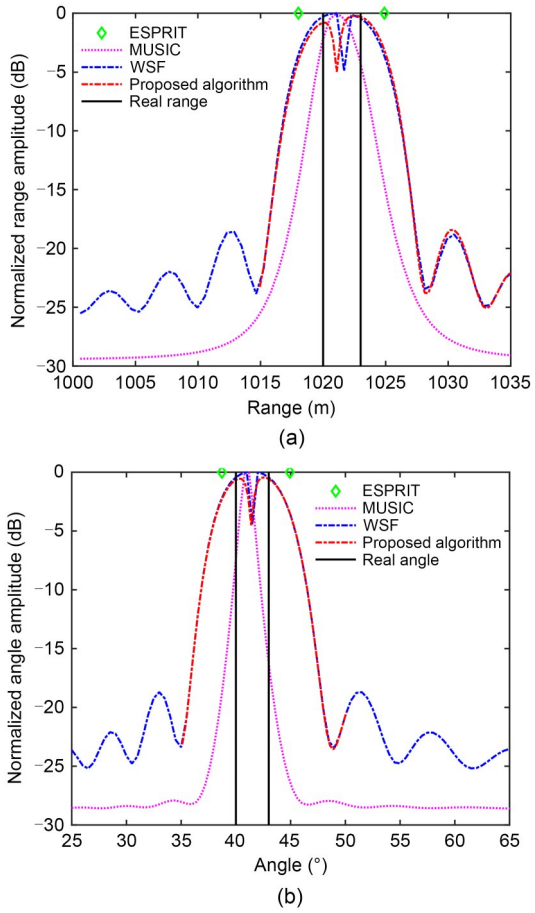

Fig. 8 Range (a) and angle (b) resolution cross-sections

angle have been updated with the coarse measurement result as the center, after which the search grid has been further subdivided to obtain accurate estimates of the angle and range using the WSF algorithm. The theoretical analysis and simulation findings demonstrated that the proposed algorithm decreases the computational cost while ensuring the estimation accuracy and resolution. In our future work, we will investigate how to combine the shape, appearance, and behavioral characteristics of targets with angle and distance information to achieve more comprehensive target recognition and classification while maintaining security and privacy. This is important for applications such as autonomous driving and security surveillance.

Contributors

Zhenkai ZHANG designed the research. All the authors performed the simulations. Xiaoke SHANG and Yue XIAO drafted the paper. Zhenkai ZHANG revised the paper. All the authors read and approved the final version.

Conflict of interest

All the authors declare that they have no conflict of interest.

Data availability

The data that support the findings of this study are available from the corresponding author upon reasonable request.

References

Dokhanchi SH, Mysore BS, Mishra KV, et al., 2019. A mmWave automotive joint radar-communications system. *IEEE Trans Aerosp Electron Syst*, 55(3):1241-1260. https://doi.org/10.1109/taes.2019.2899797

Farhang A, RezazadehReyhani A, Doyle LE, et al., 2018. Low complexity modem structure for OFDM-based orthogonal time frequency space modulation. *IEEE Wirel Commun Lett*, 7(3):344-347. https://doi.org/10.1109/lwc.2017.2776942

Franken GEA, Nikookar H, van Genderen P, 2006. Doppler tolerance of OFDM-coded radar signals. European Radar Conf, p.108-111. https://doi.org/10.1109/EURAD.2006.280285

Gaudio L, Kobayashi M, Caire G, et al., 2020a. On the effectiveness of OTFS for joint radar parameter estimation and communication. *IEEE Trans Wirel Commun*, 19(9):5951-5965. https://doi.org/10.1109/twc.2020.2998583

Gaudio L, Kobayashi M, Caire G, et al., 2020b. Joint radar target detection and parameter estimation with MIMO OTFS. IEEE Radar Conf, p.1-6. https://doi.org/10.1109/RadarConf2043947.2020.9266546

Hadani R, Rakib S, Tsatsanis M, et al., 2017a. Orthogonal time frequency space modulation. IEEE Wireless Communications and Networking Conf, p.1-6. https://doi.org/10.1109/WCNC.2017.7925924

Hadani R, Rakib S, Molisch AF, et al., 2017b. Orthogonal time frequency space (OTFS) modulation for millimeter-wave communications systems. IEEE MTT-S Int Microwave Symp, p.681-683. https://doi.org/10.1109/MWSYM.2017.8058662

Hakobyan G, Yang B, 2018. A novel intercarrier-interference free signal processing scheme for OFDM radar. *IEEE Trans Veh Technol*, 67(6):5158-5167. https://doi.org/10.1109/tvt.2017.2723868

Hassanien A, Amin MG, Aboutanios E, et al., 2019. Dual-function radar communication systems: a solution to the spectrum congestion problem. *IEEE Signal Process Mag*, 36(5):115-126. https://doi.org/10.1109/msp.2019.2900571

Keskin MF, Wymeersch H, Alvarado A, 2021. Radar sensing with OTFS: embracing ISI and ICI to surpass the ambiguity barrier. IEEE Int Conf on Communications Workshops, p.1-6. https://doi.org/10.1109/ICCWorkshops50388.2021.9473534

Li SY, Yuan WJ, Liu C, et al., 2022. A novel ISAC transmission framework based on spatially-spread orthogonal time frequency space modulation. *IEEE J Sel Areas Commun*, 40(6):1854-1872. https://doi.org/10.1109/jsac.2022.3155538

Li YC, Wang XD, Ding ZG, 2020. Multi-target position and

velocity estimation using OFDM communication signals. *IEEE Trans Commun*, 68(2):1160-1174. https://doi.org/10.1109/tcomm.2019.2956928

Liu CW, Liu SH, Mao ZH, et al., 2021. Low-complexity parameter learning for OTFS modulation based automotive radar. IEEE Int Conf on Acoustics, Speech and Signal Processing, p.8208-8212. https://doi.org/10.1109/ICASSP39728.2021.9414107

Ottersten B, Viberg M, Kailath T, 1992. Analysis of subspace fitting and ML techniques for parameter estimation from sensor array data. *IEEE Trans Signal Process*, 40(3):590-600. https://doi.org/10.1109/78.120802

Ottersten B, Viberg M, Stoica P, et al., 1993. Exact and large sample maximum likelihood techniques for parameter estimation and detection in array processing. In: Haykin S, Litva J, Shepherd TJ (Eds.), Radar Array Processing. Springer, Berlin, p.99-151. https://doi.org/10.1007/978-3-642-77347-1_4

Patole SM, Torlak M, Wang D, et al., 2017. Automotive radars: a review of signal processing techniques. *IEEE Signal Process Mag*, 34(2):22-35. https://doi.org/10.1109/msp.2016.2628914

Rahman ML, Zhang JA, Huang XJ, et al., 2020. Joint communication and radar sensing in 5G mobile network by compressive sensing. *IET Commun*, 14(22):3977-3988. https://doi.org/10.1049/iet-com.2020.0384

Raviteja P, Phan KT, Hong Y, et al., 2019a. Orthogonal time frequency space (OTFS) modulation based radar system. IEEE Radar Conf, p.1-6. https://doi.org/10.1109/RADAR.2019.8835764

Raviteja P, Hong Y, Viterbo E, et al., 2019b. Practical pulse-shaping waveforms for reduced-cyclic-prefix OTFS. *IEEE Trans Veh Technol*, 68(1):957-961. https://doi.org/10.1109/TVT.2018.2878891

Sanson JB, Tomé PM, Castanheira D, et al., 2020. High-resolution delay-Doppler estimation using received communication signals for OFDM radar-communication system. *IEEE Trans Veh Technol*, 69(11):13112-13123. https://doi.org/10.1109/tvt.2020.3021338

Shi WT, Zhang QF, He CB, et al., 2019. Taylor expansion MUSIC method for joint DOD and DOA estimation in a bistatic MIMO array. *Front Inform Technol Electron Eng*, 20(6):842-848. https://doi.org/10.1631/FITEE.1700657

Surabhi GD, Ramachandran MK, Chockalingam A, 2019a. OTFS modulation with phase noise in mmWave communications. IEEE 89th Vehicular Technology Conf, p.1-5. https://doi.org/10.1109/VTCSpring.2019.8746382

Surabhi GD, Augustine RM, Chockalingam A, 2019b. Peak-to-average power ratio of OTFS modulation. *IEEE Commun Lett*, 23(6):999-1002. https://doi.org/10.1109/lcomm.2019.2914042

Wang XJ, Zhang ZK, Najafabadi HE, 2021. Joint range and velocity estimation for integration of radar and communication based on multi-symbol OFDM radar pulses. *IET Radar Sonar Navig*, 15(5):533-545. https://doi.org/10.1049/rsn2.12071

Xue JR, Wang D, Du SY, et al., 2017. A vision-centered multi-sensor fusing approach to self-localization and obstacle perception for robotic cars. *Front Inform Technol Electron Eng*, 18(1):122-138. https://doi.org/10.1631/FITEE.1601873

Yan JK, Pu WQ, Zhou SH, et al., 2020. Collaborative detection and power allocation framework for target tracking in multiple radar system. *Inform Fus*, 55:173-183. https://doi.org/10.1016/j.inffus.2019.08.010

Zhang FQ, Zhang ZH, Yu WX, et al., 2020. Joint range and velocity estimation with intrapulse and intersubcarrier Doppler effects for OFDM-based RadCom systems. *IEEE Trans Signal Process*, 68:662-675. https://doi.org/10.1109/tsp.2020.2965820

Zhang ZK, Najafabadi HE, Jin B, 2021. Transmit array resource allocation for radar and communication integration system. *Measurement*, 173:108595. https://doi.org/10.1016/j.measurement.2020.108595

Zheng L, Wang XD, 2017. Super-resolution delay-Doppler estimation for OFDM passive radar. *IEEE Trans Signal Process*, 65(9):2197-2210. https://doi.org/10.1109/tsp.2017.2659650

Zheng L, Lops M, Eldar YC, et al., 2019. Radar and communication coexistence: an overview: a review of recent methods. *IEEE Signal Process Mag*, 36(5):85-99. https://doi.org/10.1109/msp.2019.2907329